Inorg. Chem. **2008**, *47*, 3594−3602

Cation Substitution Effects in the System $Sr_{2-x}Ba_xBi_3$ ($0 \leq x \leq 1.3$): Structural Distortions Induced by Chemical Pressure

Sung-Jin Kim, Simeon Ponou, and Thomas F. Fässler*

Department of Chemistry, Technische Universität München, Lichtenbergstrasse 4, D-85747 Garching, Germany

Received October 5, 2007

Crystals of the composition $Sr_{2-x}Ba_xBi_3$ ($0 \leq x \leq 1.3$) have been synthesized from the elements and were characterized by single-crystal and powder X-ray diffraction methods. The compounds crystallize for $x = 0$, 0.45, 0.86, 1.08, 1.28 in the structure type of the parent compound Sr_2Bi_3 with space group *Pnna* (No. 52) and $Z = 4$. Substitution of Sr by Ba leads to a site preference for Ba. The anionic Bi substructures in the pseudoternary system simultaneously distort under remarkable elongation of one distinct Bi−Bi contact. Magnetic measurements for samples with $x = 0$, 0.45 and 1.08 reveal superconducting transitions at low temperatures. Linear muffin-tin orbital band structure calculations of Sr_2Bi_3 show strong cation–anion interactions that greatly stabilize the structure. Besides showing characteristics of a typical metal, the band structure plot unveils the coinstantaneous occurrence of flat and steep bands around the Fermi level indicative for superconductivity.

Introduction

The classical Zintl–Klemm[1] concept is very useful for rationalizing and predicting the crystal structures of a wide range of solid-state compounds. Assuming complete charge transfer from the electropositive alkali (A) or alkaline-earth metal (Ae) to group 13 to group 15 metals, the bonding idea of the anionic part derives from the octet rule in molecular chemistry. However, often this approximation, that is, the mere formation of classical $2c-2e$ bonds or electron lone pairs can fail, especially in the presence of highly charged cations or small differences in electronegativity as they can occur between A or Ae metals and group 13 to the group 15 elements. Also delocalized bonding schemes can be more appropriate.[2,3] Intermetallic systems, namely, between s-block metals and metallic p-block elements often require an extension of the Zintl concept because of far more diverse and complex structures and bonding situations. Therefore, bonding in such intermetallic compounds is intermediate between semiconducting Zintl phases and s−p bonded metallic systems with completely delocalized bonding electrons. Additionally, other factors, such as optimization of Madelung energy, space filling, and the often underestimated effect of covalent interactions between electropositive and more electronegative elements, must be considered.[4–7]

The alkaline-earth bismuthides are good candidates to show this interesting interplay between various bond types. On the one hand, the pnictide-richest compounds such as cubic $SrBi_3$[8] ($AuCu_3$-type) and tetragonal $BaBi_3$[8] (distorted $AuCu_3$-type) represent pure intermetallic compounds; on the other hand, electron precise Zintl phases such as tetragonal $Ae_{11}Bi_{10}$ ($Ho_{11}Ge_{10}$ structure type) with square Bi_4^{4-} units (d(Bi−Bi) = 3.28 to 3.29 Å) and Bi_2^{4-} dumbbells (d(Bi−Bi) = 3.15 and 3.19 Å) exist for Ae = Ca, Sr, Ba.[9] However, many bismuthides show deviations when applying simple electron counting rules and have to be discussed in a more diverse way. The structures on the Ae-richer side can be traced back to Zintl-type compounds but with extra (metallic) electrons, such as tetragonal Ae_2Bi (Ae = Ca, Sr, Ba; La_2Sb

* To whom correspondence should be addressed. E-mail: thomas.faessler@lrz.tum.de.

(1) (a) Zintl, E. *Angew. Chem.* **1939**, *52*, 1. (b) Klemm, W. *Proc. Chem. Soc., London* **1959**, 329. (c) Busmann, E. *Z. Anorg. Allg. Chem.* **1961**, *313*, 90.
(2) Wade, K. *Adv. Inorg. Chem. Radiochem.* **1976**, *18*, 1.
(3) (a) Papoian, G. A.; Hoffmann, R. *Angew. Chem., Int. Ed.* **2000**, *39*, 2408. (b) Nesper, R. *Prog. Solid State Chem.* **1990**, *20*, 1.
(4) Mudring, A. V.; Corbett, J. D. *J. Am. Chem. Soc.* **2004**, *126*, 5277.
(5) Gagliardi, L.; Pyykkö, P. *Theor. Chem. Acc.* **2003**, *110*, 205.
(6) (a) Ponou, S.; Fässler, T. F.; Tobias, G.; Canadell, E.; Cho, A.; Sevov, S. C. *Chem.—Eur. J.* **2004**, *10*, 3615. (b) Ponou, S.; Kim, S.-J.; Fässler, T. F. *Z. Anorg. Allg. Chem.* **2007**, *633*, 1568.
(7) Alemany, P.; Llunell, M.; Canadell, E. *Inorg. Chem.* **2006**, *45*, 7235.
(8) Zhuravlev, N. N.; Melik-Adamyan, V. P. *Soviet Physics-Crystallography* **1961**, *6*, 99.
(9) (a) Deller, K.; Eisenmann, B. *Z. Naturforsch.* **1976**, *31B*, 29. (b) Derrien, G.; Tillard-Charbonnel, M.; Manteghetti, A. *J. Solid State Chem.* **2002**, *164*, 169.

10.1021/ic7019439 CCC: $40.75
Published on Web 03/25/2008

structure type) with isolated Bi^{3-} and one extra electron[10] or hexagonal Ae_5Bi_3 (Ae = Sr, Ba; Mn_5Si_3 structure type),[11] as well as orthorhombic Ca_5Bi_3 (Yb_5Sb_3 structure type), both again with isolated Bi^{3-} and one extra electron.[12] Electron deficient phases are observed for cubic Ae_4Bi_3 (Ae = Sr, Ba; anti Th_3P_4 structure type)[13] with formally isolated $Bi^{2.67-}$ and metallic property. Additionally, extended Bi structures such as $^1_\infty[Bi^-]$ zigzag chains and $^2_\infty[Bi^-]$ square sheets are present in orthorhombic $CaBi_2$[14] ($ZrSi_2$-type) and tetragonal $BaBi_2$[15] ($HfGa_2$-type), respectively.

As reported, the orthorhombic phase Sr_2Bi_3[14] contains infinitely extended slabs of three 3b- and two bonded 2b-Bi atoms. On the basis of a full electron transfer from strontium to the anionic network, the ionic formula splitting [(3b-Bi^0)$_2$(2b-Bi^-)] exceeds the required number of electrons by three. Recently, we reported about Ba_2Bi_3[16] that crystallizes in the W_2CoB_2 structure type. The anionic substructure there shows a layered structure with planar two-dimensional $(4.6.4.6)(4.6^2)_2$ nets with 4b- and 3b-Bi atoms. A local description of the chemical bond is possible using a nonclassical bond model and involves one extra (metallic) electron. So, in contrast to the majority of other Ae pnictides that involve polyanionic networks, the bonding and structure change dramatically by altering the Ae metal in the Ae_2Bi_3 (Ae = Sr, Ba) structure. In contrast to the features in Ba_2Bi_3, Sr_2Bi_3 contains a one-dimensional Bi polymer and represents an interesting case study of how the interplay between electronic factors, such as cation–anion interactions, and cation size determine the structure and bonding of such borderline polar intermetallic compounds.

Here we present structural changes of the known phase Sr_2Bi_3 by successive substitution of Sr by its heavier homologue Ba. Synthesis and structure refinements of new ternary compounds within the substituted series $Sr_{2-x}Ba_xBi_3$ along with theoretical bonding analysis and results of magnetic measurements are reported.

Experimental Section

Syntheses. Single-crystals of the composition $Sr_{2-x}Ba_xBi_3$ for x = 0, 0.45, 0.86, 1.08, and 1.28 were obtained from stoichiometric sample loadings $Sr_{2-y}Ba_yBi_3$ with y = 0, 0.4, 0.8, 1.0, and 1.2, respectively. To distinguish between the crystallographically determined composition and the stoichiometry of powdered samples we introduced two parameters x and y. For reactions, the pure elements were handled in an Ar-filled glovebox (O_2 and H_2O levels < 0.1 ppm). Sr (pieces, 99%, ABCR), Ba (rods, 99.3%, Chempur) and Bi (granules, 99.99%, Chempur) were weighted into Nb ampoules and sealed under reduced Ar pressure. The crucibles were subsequently enclosed in evacuated silica tubes, heated to 850 °C at a rate of 2 K·min^{-1}, slowly cooled (0.1 K·min^{-1}) to 550 °C, and annealed at this temperature for 5 days. The crystalline products exhibit metallic luster and are air sensitive. Reactions in Ta containers were performed using the same procedures.

X-ray Diffraction Experiments. Products of samples loaded as $Sr_{2-y}Ba_yBi_3$ (y = 0, 0.2, 0.4, 0.8, 1.0, 1.2) were identified by X-ray powder diffraction in Debye-Scherrer mode on an STOE STADI powder diffractometer equipped with a position sensitive detector (PSD) using Cu Kα radiation (λ = 1.540598 Å). Because of high absorption, the capillary samples were diluted with glass and measured with diamond powder as internal standard. The patterns (Supporting Information Figure 1) where indexed and refined using the software package WinXPOW (STOE). Single-crystals were picked out of the reactions that were loaded with ratios Sr/Ba/Bi = $(2 - y)$:y:3 (y = 0, 0.4, 0.8, 1.0, 1.2). The crystallographically determined compositions of the single-crystals match within limits of standard deviation (3σ rule) the stoichiometry used for each synthesis. However, there is a trend to higher Ba content (Supporting Information Figure 2). The crystals were each checked for singularity and placed on a glass tip and sealed into a capillary. Reflection data sets were collected at room temperature using a Nonius κ-CCD (x = 0, 0.86), an Oxford XCalibur3 (CCD detector) (x = 0.45), and a Nonius DIP2020 (image plate, x = 1.08, 1.28) single-crystal diffractometer. All operated with Mo Kα radiation (λ = 0.71073 Å). Absorption effects were corrected by numerical absorption correction using the STOE programs X-Red and X-Shape.[17] The crystal structures were then solved by direct methods and refined by full matrix least-squares on F^2 with the aid of the SHELXTL[18] program package. All four independent atomic positions (Bi1, Bi2, Ae1, Ae2) were refined with anisotropic atomic displacement parameters. For the pseudoternary phases the model significantly converged when introducing mixed occupancies in the two Ae sites. Some data collection and refinement parameters of the five measured crystals are listed in Table 1. Table 2 summarizes the corresponding atomic coordinates, and important interatomic distances are shown in Table 3. Further details of the crystal structures investigations together with powder diagrams can be obtained from the Supporting Information CIFs.

Elemental Analysis. Energy-dispersive X-ray measurements were carried out on different crystallites from each sample by use of a JEOL 5900LV scanning electron microscope. The measurements showed the presence of the expected elements and the absence of elements heavier than B with atomic concentrations that were in the range of the theoretical values.

Magnetic Properties Measurements. Magnetic susceptibility measurements were done using an MPMS XL SQUID-Magnetometer (Quantum Design). 27 mg, 50 mg, and 52 mg of samples with y = 0.0, 0.4, and 1.0, respectively were cooled in the absence of a magnetic field checked by an external Hall probe. Subsequent to the introduction of a 100 Oe field, data were taken, while the samples were warmed ("shielding") and then cooled ("Meissner"). The magnitudes of the shielding fraction indicate that the samples are in the superconducting state below T_C. Suprasil silica capillaries (5 mm diameter) served as sample holders.

(10) (a) Eisenman, B.; Schäfer, H. *Z. Naturforsch.* **1974**, *29B*, 13. (b) Xia, S.; Bobev, S. *J. Alloys Compd.* **2007**, *427*, 67. (c) Martinez, M.; Haase, A.; Brauer, G. *Acta Crystallogr.* **1974**, *30B*, 2003.
(11) Eisenmann, B.; Deller, K. *Z. Naturforsch.* **1975**, *30B*, 66.
(12) Martinez, M.; Haase, A.; Brauer, G. *Acta Crystallogr.* **1974**, *30B*, 2004.
(13) Li, B.; Mudring, A. V.; Corbett, J. D. *Inorg. Chem.* **2003**, *42*, 6940.
(14) Merlo, F.; Fornasini, M. L. *Mater. Res. Bull.* **1994**, *29*, 149.
(15) (a) Ponou, S.; Fässler, T. F. *Zintl phases with Hypervalent bonding in Alkaline-Earth Bismuthides, Binary systems ABi_2 (A = Ca, Ba)*; GDCh-Jahrestagung, München, Okt. 2003; abstract book, p 168. (b) Ponou, S. Dissertation, Technische Universität München, 2006, Germanides, Germanide-Tungstate Double Salts and Substitution Effects in Zintl Phases.
(16) Ponou, S.; Fässler, T. F. *Inorg. Chem.* **2004**, *43*, 6124.
(17) (a) *X-RED: Stoe Data Reduction Program*, Version 1.22; Stoe & Cie GmbH: Darmstadt, Germany, 2001. (b) *X-Shape: Crystal Optimization for Numerical Absorption Correction*, Version 1.06; Stoe & Cie: Darmstadt, Germany, 1999.
(18) (a) Sheldrick, G. M. *SHELXS-97: Program for the Solution of Crystal Structures*; Universität Göttingen: Göttingen, Germany, 1997. (b) Sheldrick, G., *SHELXL-97: Program for the Refinement of Crystal Structures*; Universität Göttingen: Göttingen, Germany, 1997.

Table 1. Crystallographic and Structure Refinement Data for the Compounds $Sr_{2-x}Ba_xBi_3$ ($x = 0$, 0.45, 0.86, 1.08, 1.28)

empirical formula	Sr_2Bi_3 (**1**)	$Sr_{1.55}Ba_{0.45(2)}Bi_3$ (**2**)	$Sr_{1.14}Ba_{0.86(2)}Bi_3$ (**3**)	$Sr_{0.92}Ba_{1.08(4)}Bi_3$ (**4**)	$Sr_{0.72}Ba_{1.28(4)}Bi_3$ (**5**)
fw, g mol^{-1}	802.18	824.68	844.69	856.00	865.57
space group, Z			*Pnna* (No. 52), *4*		
a, Å	15.645(3)	15.745(3)	15.881(3)	15.887(3)	15.908(3)
b, Å	6.797(1)	6.829(1)	6.888(1)	6.893(1)	6.908(1)
c, Å	6.601(1)	6.647(1)	6.704(1)	6.717(1)	6.731(1)
V, Å^3	701.9(2)	714.8(2)	733.4(3)	735.6(3)	739.7(3)
μ (Mo Kα), mm^{-1}	89.92	87.41	84.41	83.72	82.89
ρ, g cm^{-3}	7.59	7.66	7.65	7.73	7.77
R_1, wR_2 [$I > 2\sigma(I)$]	0.048, 0.126	0.034, 0.076	0.032, 0.079	0.060, 0.160	0.064, 0.160
R_1, wR_2 (all data)[a,b]	0.051, 0.128	0.039, 0.078	0.041, 0.082	0.063, 0.163	0.066, 0.162
weighting scheme	$a = 0.0659$; $b = 30.68$	$a = 0.023$; $b = 21.24$	$a = 0.0515$; $b = 0$	$a = 0.0633$; $b = 149.29$	$a = 0.0513$; $b = 80.08$

[a] $R_1 = \Sigma||F_c| - |F_c||/\Sigma|F_o|$; $wR_2 = [\Sigma[w(F_o^2 - F_c^2)^2]/\Sigma[w(F_o^2)^2]]^{1/2}$. [b] $w = 1/[\sigma^2(F_o^2) + (aP)^2 + bP]$, where $P = (\mathrm{Max}(F_o^2,0) + 2F_c^2)/3$.

Table 2. Atomic Coordinates and Isotropic Equivalent Displacement Parameters[a] for $Sr_{2-x}Ba_xBi_3$ ($x = 0$, 0.45, 0.86, 1.08, 1.28)

	$x = 0$	$x = 0.45$	$x = 0.86$	$x = 1.08$	$x = 1.28$
			Bi1 (8*e*)		
x	0.3461(1)	0.3462(1)	0.3459(1)	0.3457(1)	0.3455(1)
y	0.5641(1)	0.5613(1)	0.5591(1)	0.5585(1)	0.5578(1)
z	0.0787(1)	0.0770(1)	0.0752(1)	0.0747(1)	0.0741(2)
U_{eq}	0.0209(4)	0.0245(2)	0.0214(2)	0.0232(4)	0.0287(5)
			Bi2 (4*d*)		
x	0.4293(1)	0.4307(1)	0.4313(1)	0.4313(1)	0.4313(1)
y	¼	¼	¼	¼	¼
z	¾	¾	¾	¾	¾
U_{eq}	0.0192(4)	0.0224(2)	0.0202(5)	0.0179(6)	0.0252(6)
			Sr1/Ba1 (4*c*)		
	¼	¼	¼	¼	¼
x					
y	0	0	0	0	0
z	0.9434(4)	0.9448(2)	0.9463(2)	0.9478(3)	0.9479(4)
U_{eq}	0.0179(6)	0.0196(5)	0.0130(5)	0.0168(10)	0.0212(10)
			Sr2/Ba2 (4*d*)		
x	½	½	½	½	½
y	¼	¼	¼	¼	¼
z	¼	¼	¼	¼	¼
U_{eq}	0.0200(7)	0.0191(6)	0.0145(5)	0.0169(11)	0.0237(10)

[a] $U_{eq} = 1/3(U_{11} + U_{22} + U_{33})$.

Electronic Structure Calculations. Self-consistent band structure calculations for Sr_2Bi_3, hypothetical, isopointal "Ba_2Bi_3" and for reasons of comparison for intra (3.07 Å) and interlayer (3.53 Å) Bi−Bi contacts of elemental Bi (space group $R\bar{3}m$) were performed with the linear-muffin-tin-orbital (LMTO) method using the Stuttgart LMTO47[19] program code with the Crystal Orbital Hamilton Population (COHP)[20] extension implemented. For calculations s, p, "downfolded" d, and f partial waves for Bi together with s, d, "downfolded" p, and f waves for Sr and Ba were used. Grids of 2048 irreducible k points of the first Brillouin zone were used for reciprocal space integrations performed by the tetrahedron method.[21] For bonding analysis, the energy contributions of all electronic states for selected bonds were calculated by the COHP method. Integration over all filled states gives ICOHP values which measure relative bond strengths. Negative −COHP and −ICOHP values indicate bonding interactions. The hypothetically ordered "Ba_2Bi_3" was calculated using lattice parameters of the crystal with the highest refined Ba content ($Sr_{0.72}Ba_{1.28(4)}Bi_3$) and fully occupying both Sr sites (4*c*, 4*d*) with Ba.

Results

Description of the Crystal Structure of Sr_2Bi_3. The compound Sr_2Bi_3 crystallizes in the orthorhombic space group *Pnna* (No.52) with Pearson code *oP*20. The structure determination validates the results of Merlo and Fornasini.[14] Lattice parameters and structure refinement details are identical within standard deviations and are presented here again for reason of comparison with the substitution variants. As described in the original publication, the Bi atoms form a two-dimensional slab in the b and c directions with 3b- and 2b-Bi atoms (Figure 1a,b) and three different homoatomic distances b_1:= d(Bi1−Bi1) = 3.132(1) Å, b_2:= d(Bi1−Bi2) = 3.310(1) Å, and b_3:= d(Bi1−Bi1) = 3.392(1) Å. Regarding the Bi substructure and taking into account only the shortest Bi−Bi contacts b_1, Bi_2 dumbbells of Bi1 atoms and isolated atoms of Bi2 result. The dumbbells are aligned along [100] and tilted in the *ab* plane by 16.2°. They are connected to four other dumbbells via direct contacts (b_3) or bridging Bi2 atoms, which form b_2-type contacts. Each Bi1 atom of the dumbbells forms one b_3 contact to a neighboring dumbbell and one b_2 contact to Bi2 atoms (b_2 and b_3 are mean oriented along [011] and [01–1]).

Another view of the Bi substructure arises by regarding the shorter b_1 and b_2 contacts resulting in a one-dimensional, helical Bi substructure. The spirals have six atoms per turn (4x Bi1, 2x Bi2) and proceed along [010] (Figure 1c,d). Those chains are interlinked in the c direction by longer b_3 contacts between Bi1 atoms of different helices, resulting in two-dimensional Bi slabs in the *bc* plane (Figure 1b,e). The Bi−Bi separation between the slabs are 3.902(1) Å. The interatomic distance b_1 is longer than the one observed in elemental Bi (3.07 Å, intralayer distance) but is in the range of $2c-2e$ covalent bonds as found, for example, for Bi_2^{4-} dumbbells in $Sr_{11}Bi_{10}$ (3.19 Å). The distances b_2 and b_3 are longer than $2c-2e$ bond lengths and are typical for multicenter bonding as it is observed in the two-dimensional Bi net in Ba_2Bi_3, where Bi−Bi distances range from 3.25 to 3.38 Å or the six-atom-wide Bi ribbon found in $HfBi_2$[22] with Bi−Bi separations of 3.28 Å. Those interactions are longer than typical covalent bonds. However, considering the coordination number of Bi1, we still assume some degree of directive chemical bonding to Bi2. Sr1 atoms with

(19) (a) Andersen, O. K. *Phys. Rev. B* **1975**, *12*, 3060. (b) Anderson, O. K.; Jepsen, O. *Phys. Rev. Lett.* **1984**, *53*, 2571.
(20) Blöchl, P. E.; Dronskowski, R. *J. Phys. Chem.* **1993**, *97*, 8617.
(21) Blöchl, P. E.; Jepsen, O.; Andersen, O. K. *Phys. Rev. B* **1994**, *49*, 16223.
(22) Haase, M. G.; Block, H.; Jeitschko, W. *Z. Anorg. Allg. Chem.* **2001**, *627*, 1941.

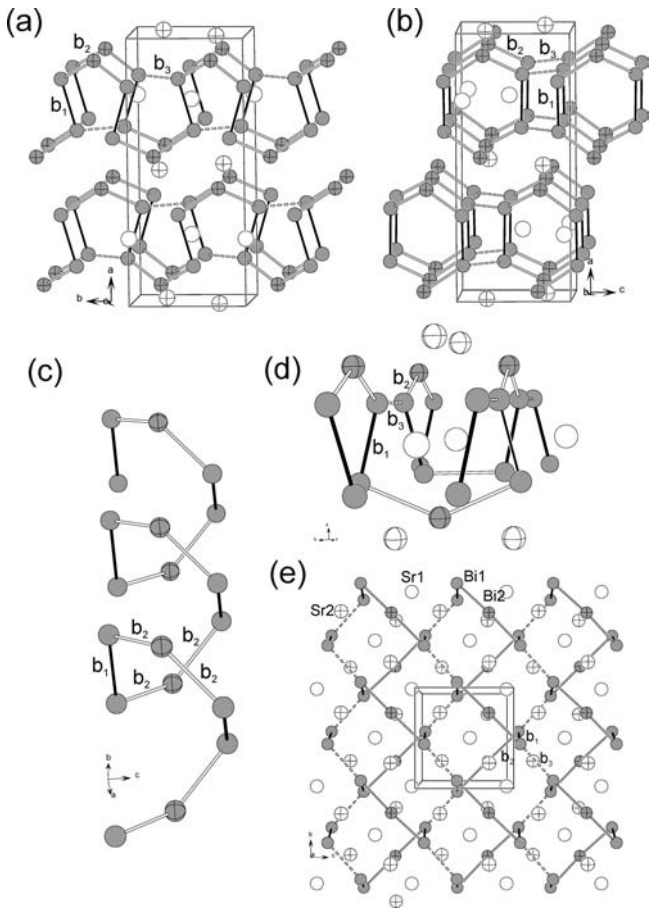

Figure 1. Structure of Sr_2Bi_3 in a projection (a) along [001] and (b) along [010]; (c) the 2D-Bi slab can be alternatively described as an interconnection of the depicted Bi spiral ([110]-view); (d) perspective view with Sr1 atoms centering the Bi dumbbells; (e) central projection along [100] of the Bi slab and embedded cations. Sr1 (white), Sr2 (white, cross hatched), Bi1 (gray), and Bi2 (gray, cross hatched). Bi−Bi contacts b_1, b_2, and b_3 are drawn as solid, open, and dashed lines, respectively.

Wyckoff position 4*c* are distributed in layers in the *bc* plane with *x* coordinates centering b_1 of the Bi1 dumbbells along [100]. Sr2 atoms with Wyckoff position 4*d* are also distributed in layers in the *bc* plane and separate the 2D-Bi slabs along [100] (Figure 1a,b). Sr1 resides approximately in the center of four Bi1 dumbbells (Figure 1e) with Sr1−Bi1 distances of 3.440(1), 3.521(1), 3.787(3), and 4.214(1) Å. The coordination sphere is completed by two Bi2 atoms connecting three of the four Bi_2 dimers with Sr1−Bi2 distance of 3.519(1) Å (Figure 2a). An average Sr−Bi distance of 3.582 Å results, if only distances up to 4 Å are considered. The high coordination number of the Sr1 site by Bi1 is significant in the bonding considerations, as will be described later. As shown in Figure 2b, the Sr2 coordination consists of a polyhedron with eight Bi atoms: four Bi1 atoms (d(Sr2−Bi1) = 3.409(2) and 3.479(2) Å) of the dumbbells and four bridging Bi2 atoms (d(Sr2−Bi2) = 3.481(1) and 3.575(1) Å) generate a rectangular antiprism with average Sr−Bi distance of 3.486 Å. One rectangular face is defined by b_2 contacts of two different helical chains and longer b_4 contacts of 3.902(1) Å between Bi1 and Bi2 atoms that are part of two different 2D-slabs. The resulting polyhedra are base fused and piled to columns in the [01–1] direction (Figure 2c).

Crystal Structure of $Sr_{2-x}Ba_xBi_3$ (x = 0.45, 0.86, 1.08, 1.28). Incremental increase of the Ba content in steps of 0.2 in the system $Sr_{2-x}Ba_xBi_3$ leads to an increase in the lattice parameters (Figure 3). Because of the bigger size of Ba compared to the size of Sr, such enlargement of the unit cell dimensions is expected on substitution. Following Vegard's rule, the increase is approximately linear from x = 0 to 0.8, and a decreasing gradient from 0.8 to 1.2 is observed. Lattice parameters, calculated from powder diffractograms show that the *a*, *b*, and *c* axes increase by 1.93%, 1.60%, and 1.91%, respectively. In other words, the expansion occurs almost uniformly in all three dimensions by approximately 2% but is slightly less pronounced along the *b* direction. The cell volume is increased by 5.56%. The lattice expansion correlates directly with anisotropic changes in interatomic distances as discussed in the following. Single-crystals were obtained from the reactions with starting stoichiometries $Sr_{2-y}Ba_yBi_3$ and y = 0.4, 0.8, 1.0, and 1.2.

Table 3. Interatomic Distances (up to 4 Å) within the Compounds $Sr_{2-x}Ba_xBi_3$ for x = 0, 0.45, 0.86, 1.08, and 1.28 and Largest Distance Change

atom 1	atom 2	x = 0	x = 0.45	x = 0.86	x = 1.08	x = 1.28	$d_{(x=1.28)} - d_{(x=0)}$
Sr1	Bi1 2x	3.440(1)	3.469(1)	3.506(1)	3.506(2)	3.515(1)	0.07
	Bi2 2x	3.519(1)	3.562(2)	3.604(1)	3.612(2)	3.617(2)	0.10
	Bi1 2x	3.521(3)	3.545(1)	3.574(1)	3.569(3)	3.577(3)	0.06
	Bi1 2x	3.787(3)	3.808(1)	3.835(1)	3.849(3)	3.853(3)	0.06
Sr2	Bi1 2x	3.409(2)	3.424(1)	3.454(1)	3.457(2)	3.462(2)	0.05
	Bi1 2x	3.479(2)	3.498(1)	3.526(1)	3.532(2)	3.541(2)	0.06
	Bi2 2x	3.481(1)	3.499(1)	3.527(1)	3.533(1)	3.540(1)	0.06
	Bi2 2x	3.575(1)	3.584(1)	3.611(1)	3.613(1)	3.621(1)	0.05
Bi1	Bi1 (b_1)	3.132(1)	3.142(1)	3.154(1)	3.145(2)	3.142(2)	0.01
	Bi2 (b_2)	3.310(1)	3.319(1)	3.336(1)	3.337(2)	3.339(1)	0.03
	Bi1 (b_3)	3.392(1)	3.454(1)	3.523(1)	3.537(2)	3.557(2)	0.17
	Sr2	3.409(2)	3.424(1)	3.454(1)	3.457(2)	3.462(2)	0.05
	Sr1	3.440(1)	3.469(1)	3.506(1)	3.506(2)	3.515(1)	0.07
	Sr2	3.479(2)	3.498(1)	3.526(1)	3.532(2)	3.541(2)	0.06
	Sr1	3.521(3)	3.545(1)	3.574(1)	3.579(3)	3.577(3)	0.06
	Sr1	3.787(3)	3.808(1)	3.835(1)	3.849(3)	3.853(3)	0.06
	Bi2	3.902(1)	3.915(1)	3.952(1)	3.959(2)	3.971(2)	0.07
Bi2	Bi1 2x	3.310(1)	3.319(1)	3.336(1)	3.337(2)	3.339(1)	0.03
	Sr2 2x	3.481(1)	3.499(1)	3.527(1)	3.533(1)	3.540(1)	0.06
	Sr1 2x	3.519(1)	3.562(1)	3.604(1)	3.612(2)	3.617(2)	0.10
	Sr2 2x	3.575(1)	3.584(1)	3.611(1)	3.613(1)	3.621(1)	0.05
	Bi1 2x	3.902(1)	3.915(1)	3.952(1)	3.959(2)	3.971(2)	0.07

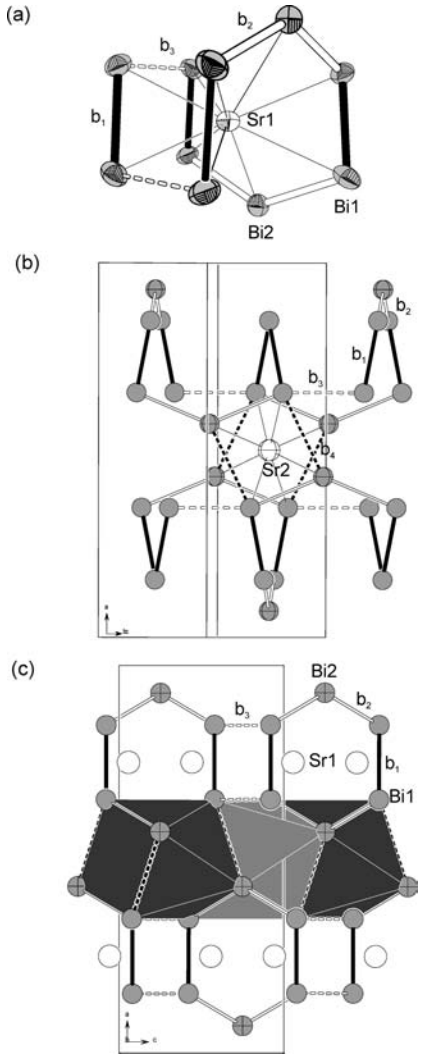

Figure 2. Coordination spheres around (a) Sr1 (ellipsoids at 90%) and (b) Sr2. The stacking of the rectangular antiprisms around Sr2 in the unit cell is shown in (c). Sr1 (white), Sr2 (white, crossed), Bi1 (gray), and Bi2 (gray, crossed); the shortest Bi−Bi contact is drawn as solid and the longer ones are drawn as open and dashed lines.

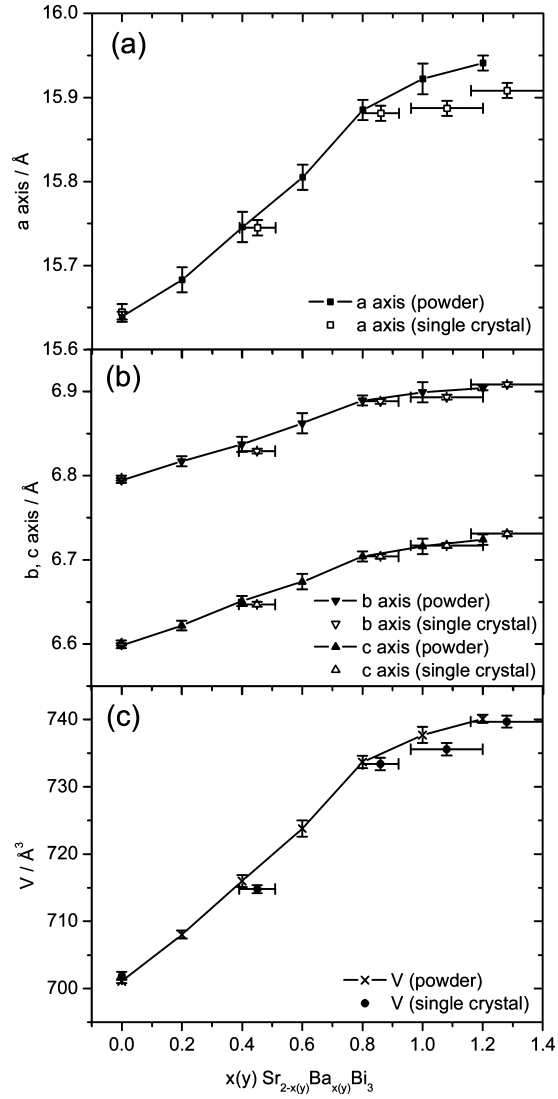

Figure 3. Lattice parameters (*a, b, c, V*) obtained from X-ray powder and single-crystal diffraction. Error bars are $\pm 3\sigma$ of the values; for values, see Table 5.

Important crystal data are given in Tables 1 and 2, and important distances are listed in Table 3. All refinements were carried out using the space group and atomic positions of Sr_2Bi_3. No reflections indicating a superstructure were observed. Samples with Ba loading higher than $y = 1.0$ show lower crystallinity and are less homogeneous. In the corresponding powder diagrams, the presence of additional reflections indicates the formation of an unknown phase. Therefore, we did not investigate the systematic substitution properties of $Sr_{2-y}Ba_yBi_3$ beyond $y = 1.2$. Lattice parameter determination and refinement with partial Ba occupation on the Sr positions reveal that the compositions of the single-crystals confirm within standard deviations (3σ rule) the results of the powder X-ray studies. Lattice parameters determined from single-crystals and from powder data nearly coincide with exceptions for the samples loaded as $y = 1.0$ and 1.2 (Figure 3). In these cases, the *a* lattice parameter determined from the powdered samples are slightly longer than the one identified from the single-crystals with $x = 1.08(4)$ and 1.28(4), respectively.

The degree of Sr substitution with Ba is not equally distributed over the two sites Sr1 and Sr2. In all cases we find a higher Ba content on the Sr1 than on the Sr2 position. Figure 4 and Table 4 clearly show that Ba is preferably substituted in the 4*c* (Sr1) position at lower Ba contents. On the basis of the crystallographically determined compositions for $x = 0.45(2)$, we find approximately 35% Ba on Sr1 compared to 10% on the Sr2 position, and for $x = 1.28(4)$, approximately 75% and 53%, respectively. This trend reflects the situation of a larger coordination sphere of Sr1 with coordination number 10 and longer mean Sr−Bi distance compared to that of Sr2.

The enlargement of the lattice parameters from Sr_2Bi_3 to $Sr_{0.72}Ba_{1.28(4)}Bi_3$ is accompanied with a change of interatomic separations in the crystal structure (Table 3). Increasing the Ba content leads to a change of the tilt angle of the Bi_2 dumbbells in the *ab* plane (Figure 1e) with values of 15.5°, 15.0°, 14.9°, and 14.7° for $x = 0.45$, 0.86, 1.08, and 1.28, respectively. Even more significant is the fact that the interatomic distances change anisotropically. Certain distances remain almost unaffected, whereas others change to

Table 5. Stoichiometries of the Reactions with Unit Cell Parameters of Powdered Samples[a]

	unit cell parameters of powders					unit cell parameters of single-crystal			
stoichiometry	*a*, Å	*b*, Å	*c*, Å	*V*, Å^3	composition[b]	*a*, Å	*b*, Å	*c*, Å	*V*, Å^3
Sr_2Bi_3	15.639(2)	6.795(2)	6.598(1)	701.1(1)	Sr_2Bi_3	15.645(3)	6.797(1)	6.601(1)	701.9(2)
$Sr_{1.8}Ba_{0.2}Bi_3$	15.683(5)	6.817(5)	6.622(2)	708.0(2)					
$Sr_{1.6}Ba_{0.4}Bi_3$	15.746(6)	6.837(6)	6.651(3)	716.0(3)	$Sr_{1.55}Ba_{0.45(2)}Bi_3$	15.745(3)	6.829(1)	6.647(1)	714.8(2)
$Sr_{1.4}Ba_{0.6}Bi_3$	15.805(5)	6.862(5)	6.674(4)	723.8(4)					
$Sr_{1.2}Ba_{0.8}Bi_3$	15.885(4)	6.889(4)	6.704(2)	733.7(3)	$Sr_{1.14}Ba_{0.86(2)}Bi_3$[c]	15.887(3)	6.893(1)	6.717(1)	735.6(3)
$Sr_{1.0}Ba_{1.0}Bi_3$	15.922(6)	6.899(6)	6.716(4)	737.7(4)	$Sr_{0.92}Ba_{1.08(4)}Bi_3$	15.881(3)	6.888(1)	6.704(1)	733.4(3)
$Sr_{0.8}Ba_{1.2}Bi_3$	15.941(3)	6.904(3)	6.724(1)	740.1(2)	$Sr_{0.72}Ba_{1.28(4)}Bi_3$	15.908(3)	6.908(1)	6.731(1)	739.7(3)

[a] The crystallographically determined compositions of corresponding single-crystals together with unit cell parameters are shown at the right-hand side. [b] Composition of single-crystals. [c] Single-crystal isolated from loaded stoichiometry Sr/Ba/Bi = 1: 1: 3.3.

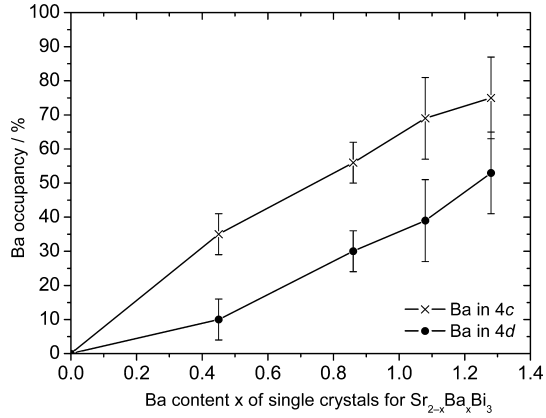

Figure 4. Occupancy of Ba in the 4*c* and 4*d* position in substituted $Sr_{2-x}Ba_xBi_3$ plotted against Ba content. Error bars are ±3 σ of the values.

Table 4. Occupancy of Ba in the (4*c*) and (4*d*) Position in Substituted $Sr_{2-x}Ba_xBi_3$ (x = 0–1.28) and Shortest Bi−Bi Distances (b_3) between Two Adjacent Bi Spirals

x	occ. (%) Ba in 4*c*	occ. (%) Ba 4*d*	b_3 = *d*(Bi1−Bi1), Å
0	0	0	3.392(1)
0.45	35	10	3.454(1)
0.86	56	30	3.523(1)
1.08	69	39	3.537(2)
1.28	75	53	3.557(2)

a greater extent. While the shorter distances b_1 and b_2 remain almost unaltered, with 3.132(1) to 3.142(2) Å for b_1 and 3.310(1) to 3.339(1) Å for b_2, the longer b_3 contact increases from 3.392(1) to 3.557(2) Å for x = 0 to 1.28(4), respectively. The larger expansion of the interspiral bond b_3 by approximately 5% compared with the other Bi−Bi contacts, which are enlarged by less than 1%, originates from the site preference of Ba on the Sr1 position. This pushes two adjacent $(Bi1)_2$ dumbbells that are coordinated by the same Sr1 atom apart from each other (Figures 1d and 2a). The final b_3 distance of 3.557(2) Å lies in the region of the Bi−Bi contacts of interlayer Bi−Bi distances in elemental bismuth (3.53 Å) and contacts in $BaBi_3$ (3.66 Å). This indicates loss of the directional interaction and a shift to a more electronically delocalized system.

The cation–anion separations disclose another feature of the structure. Whereas for x = 0 the distances Ae1−Bi1, Ae2−Bi2, and Ae2−Bi1 are longer (3.409(2) to 3.481(1) Å) than b_3 (3.392(1) Å), the situation is reversed for x = 1.28(4) Å, where the heteratomic distances of 3.462(2) to 3.541(2) Å are shorter than b_3 with a value of 3.557(2) Å. This clearly indicates a weakening (elongation) of the

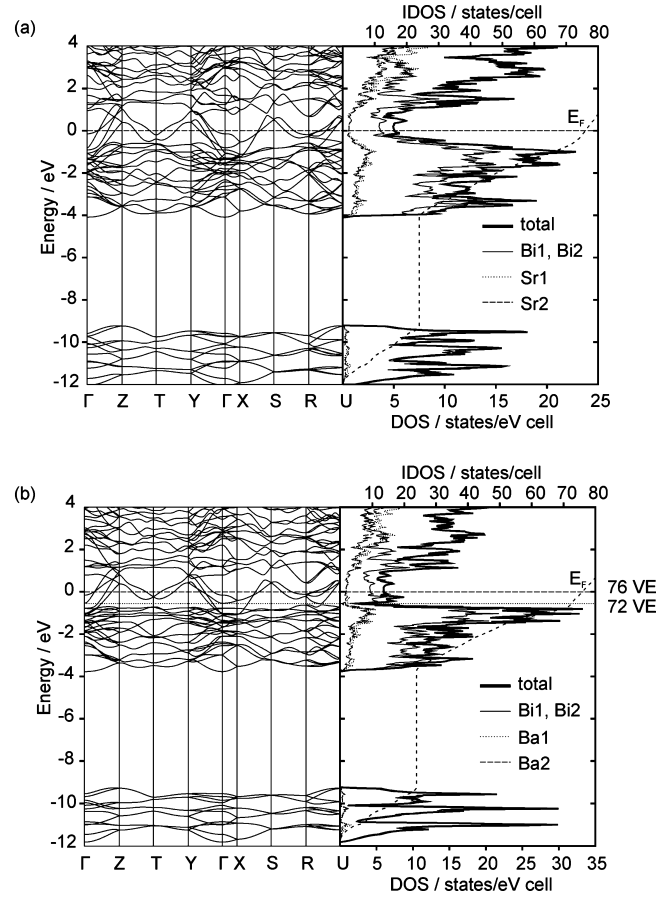

Figure 5. Band structures and total and projected DOS plots, calculated with the LMTO method, for (a) Sr_2Bi_3 and (b) for the hypothetical phase "Ba_2Bi_3".

homoatomic contact b_3 when compared to the contacts between positively and negatively charged atoms. This result can geometrically be interpreted as a simultaneous separation and stretching of the Bi helices along [010].

Electronic Structure. To gain deeper insights into the complex electronic situation of Sr_2Bi_3 and the effects of Ba substitution, that is, the cation–anion interactions, computational calculations were carried out. The band structure of Sr_2Bi_3 along specific symmetry paths of the primitive orthorhombic Brillouin zone and the total density of states together with the projected density of states (DOS) for Sr and Bi are depicted in Figure 5a. Various bands cross the Fermi level and mark Sr_2Bi_3 as an isotropic conductor. As revealed by fat band representations, bands that cross E_F with large dispersions have mainly Bi-p character (Supporting Information Figure 3). A local maximum just below E_F is

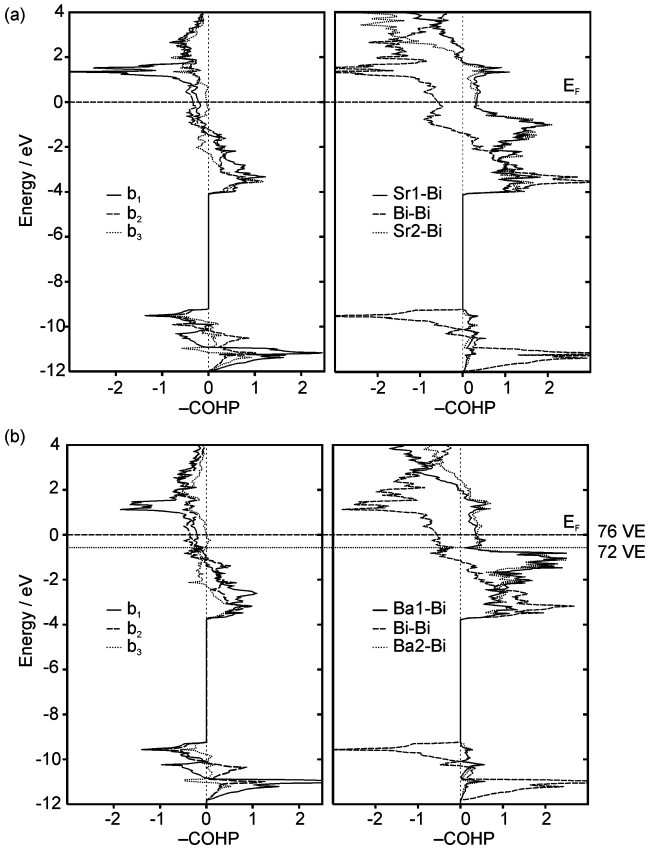

Figure 6. −COHP plots for (a) Sr_2Bi_3 and (b) "Ba_2Bi_3"; left, the three separate Bi−Bi pairs (b_1 (line), b_2 (dashed), b_3 (dotted)); right, the sum of all Bi−Bi (dashed), Ae1−Bi (line), and Ae2−Bi (dotted) interactions.

caused by flat bands at Γ, T, and R symmetry points. The projected DOS show that in an energy window of ±4 eV around E_F significant numbers of Bi-p states, with larger contributions from Bi1 according to the ratio Bi1/Bi2 = 2:1, are present. The Bi-s states are clearly separated in a band ranging from −9 and −12 eV. Sr orbitals are clearly present in the valence band and mix with Bi-p states. These sets of Sr and Bi orbitals are responsible for the metallic character of Sr_2Bi_3. Figure 6a shows the COHP diagrams of the three different Bi−Bi bonds (eV/bond) and the sums of all Bi−Bi, Sr1−Bi, and Sr2−Bi bonds. Bonding states of the different Bi−Bi interactions are filled and are located below the Fermi level. Some antibonding states are filled as well with electrons hinting for an electron rich compound. The shortest Bi1−Bi1 contact of 3.13 Å is more than twice as strong as the longest contact of 3.39 Å, which is reflected in the −ICOHP values of 1.38 and 0.49 eV/bond, respectively (Supporting Information Table 1). The values compare well with the ones calculated for elemental Bi (intralayer Bi−Bi, 1.58 eV, and interlayer Bi−Bi contacts (3.53 Å), 0.19 eV). Because antibonding Bi−Bi states are filled, Bi−Bi contacts alone appear to be too weak to control the overall structure. On the one hand, for all three contacts b_1, b_2, and b_3, the maximum −ICOHP values lie well below E_F (∼2 eV). On the other hand Ae−Bi interactions are clearly present at E_F, and the corresponding −COHP plots show a strong bonding nature with approximately equal values for Sr1−Bi and Sr2−Bi.

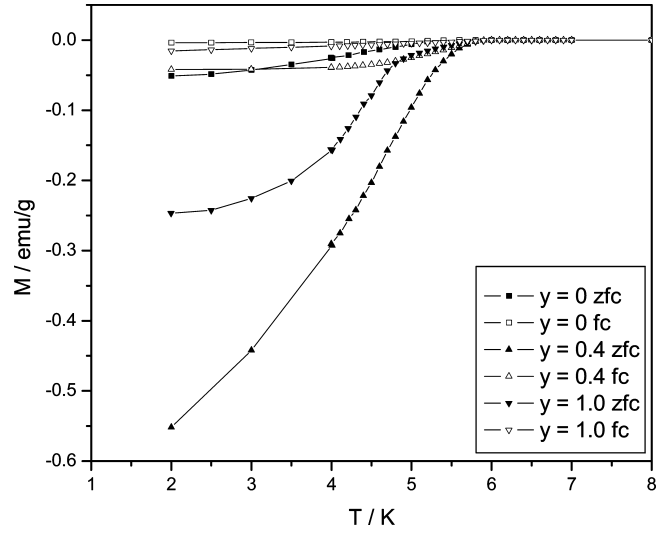

Figure 7. Diamagnetic shielding (filled symbols) and Meissner effect (open symbols) as a function of temperature for samples $Sr_{2-y}Ba_yBi_3$ with $y = 0$, 0.4, and 1.0 (100 Oe; zfc, zero-field-cooled; fc, field-cooled).

Therefore, the loss of Bi−Bi bonding is compensated by a gain of bonding interactions with the cations.

For comparison, the electronic structure of the hypothetical "Ba_2Bi_3" with Sr_2Bi_3 structure was calculated. Both Ae sites were occupied with Ba and the unit cell parameters of the Ba richest crystal $Sr_{0.72}Ba_{1.28(4)}Bi_3$, **5**, (Table 1) were used. The band structure and the DOS plots are shown in Figure 5b. Compared with the Sr compound the valence band of "Ba_2Bi_3" is slightly less dispersed, originating from less interactions because of longer interatomic distances. Replacing Sr1 by Ba and increasing the lattice parameters reveals the opening of a pseudo gap at −0.5 eV. Rigid band filling up to the pseudo gap requires 72 valence electrons for the unit cell. However, the Ba-d mixing with Bi-p does not completely open the gap, and thus the compound conserves its metallic character. The Ba−Bi and Bi−Bi COHP values for "Ba_2Bi_3" reveal a significant loss of Bi−Bi bonding character (Figure 6b).

The −ICOHP value of the weakest interaction b_3 (0.49 eV) in Sr_2Bi_3, which was in the range of the average Sr1−Bi (0.54 eV), significantly drops to 0.33 eV for "Ba_2Bi_3". The corresponding average Ba1−Bi contact was calculated to be 0.55 eV. Therefore, it can be concluded that the site preference of the cation might also be triggered by the ratio of Bi−Bi versus Ba−Bi bonding character.

Physical Properties. The temperature-dependent magnetic behavior of samples with loadings Sr_2Bi_3, $Sr_{1.6}Ba_{0.4}Bi_3$, and $Sr_1Ba_1Bi_3$ were carried out. To exclude superconducting impurities through the ampule materials, we synthesized Sr_2Bi_3 in Ta and Nb ampoules. Sr_2Bi_3 shows a transition temperature of approximately 4.4 K. The presence of elemental Ta was excluded since the curves nearly coincide with the ones from a measurement of binary Sr_2Bi_3 prepared in a Nb ampoule (Supporting Information Figure 4). Figure 7 shows the experimental diagrams of the samples with $y =$ 0, 0.4, and 1.0 synthesized in Ta containers. For the measurements, each sample was cooled without external field to 2 K. After applying a field of 100 Oe, the sample was

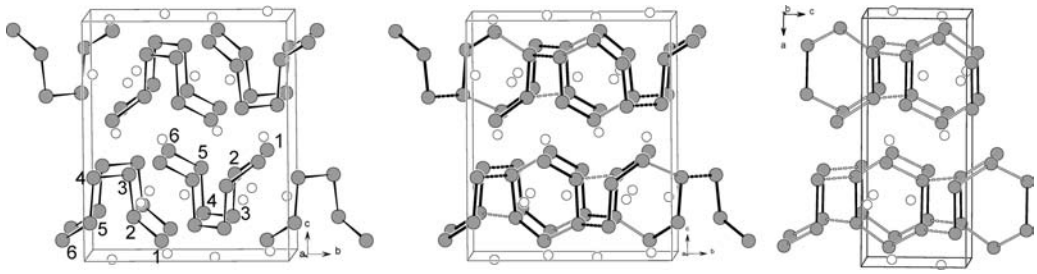

Figure 8. Schematic transition of the Sb substructure in Sr_2Sb_3 (left) to the Bi substructure of Sr_2Bi_3 (right).

heated to 10 K. At low temperatures, the samples are diamagnetic. This property disappears at higher temperatures and occurs again when cooling in the external field at a transition temperature of approximately 4.4 K. The magnitudes at 100 Oe are in the range of the magnetization values reported for other intermetallic superconductors such as $BaSn_3$ and $BaSn_5$[23] and are indicative for the bulk property of the sample. The plots have the characteristics of a type-II superconductor showing diamagnetic shielding (zero-field-cooled) and Meissner effect (field-cooled).

Discussion

Trying to apply the Zintl−Klemm concept for Sr_2Bi_3 leads to the following descriptions: (a) Bi1 dumbbells Bi_2^{4-} and isolated Bi^{3-} lead to $[(1b\text{-}Bi^{2-})_2(Bi^{3-})]$ thus ignoring b_2 and b_3 contacts results in an electron deficiency of 3 electrons; (b) the assumption of isolated spirals with two-bonded atoms only and neglecting just the longer b_3 contact results in the charge assignment $[(2b\text{-}Bi^{1-})_3]$ and one extra electron, and finally (c) according to Merlo and Fornasini, considering a three-bonded Bi1 atom leads to the charge assignment $[(2b\text{-}Bi^{1-})(3b\text{-}Bi^{0})_2]$ and three additional electrons. None of the descriptions represents a classical closed-shell bonding situation. Sr_2Bi_3 can therefore not be considered as a Zintl phase, and multicenter interactions as well as cation effects must play a crucial role to stabilize the Bi substructure. In contrast to the isoelectronic structure of Sr_2Sb_3,[24] which contains discrete six member $[Sb_6]^{8-}$ zigzag chain segments and which represents an electron-precise Zintl compound, the electronic situation in Sr_2Bi_3 is puzzling and does not follow the (8-N) rule.

As indicated in the original literature, Sr_2Bi_3 adapts a more symmetrical variant of the monoclinic Sr_2Sb_3 structures Eu_2Sb_3[25] and Ca_2As_3[26] structure. Figure 8 depicts the topological transformation of the Sr_2Sb_3 to the Sr_2Bi_3 structure by bond scission and formation. The six-member chain unit in the Zintl phase Sr_2Sb_3 [Sb1−Sb2−Sb3−Sb4−Sb5−Sb6]$^{8-}$ is split into two parts of equal length by releasing the originally longest Sb3−Sb4 bond of 3.006 Å and transforming it to a b_3-type contact. The two shortest Sb2−Sb3 and Sb4−Sb5 bonds are preserved as b_1 contacts. Weaker b_2-type contacts are established between originally not bonded Sb3 and Sb6 (and Sb1 and Sb4) atoms of adjacent six-atom units forming the one-dimensional spirals as described for Sr_2Bi_3. The transformation follows the path of a group−subgroup relationship as discussed for Eu_2Sb_3.[25] Chemically the transition of E_6^{8-} oligomers to a one-dimensional $^1_\infty[Bi_6]^{6-}$ polymer represents an oxidative coupling reaction accompanied by the loss of 2 electrons per oligomer. As outlined by the calculations, the ordered phase "Ba_2Bi_3" shows a pseudo gap corresponding to an IDOS of 72 VE per unit cell because of the larger polymer separation. In the bismuthide, electrons are weakly bound in Ae−Bi interactions, and they are therefore not available for complete charge transfer as in Sr_2Sb_3. Thus, Sr_2Bi_3 overall reaches a better electronic situation by the formation of a polymer with weakly connected dumbbells and using the excess electrons for Ae−Bi bonding. This situation suggests that interspiral Bi−Bi contacts (b_3) are less important, and that the contacts b_1 and b_2 single out a one-dimensional polymer chain. Applying the 8-N rule to a one-dimensional Bi chain formally leads to one negative charge per atom, $^1_\infty[Bi^-]$, with one transferred electron located at the Bi atom and therefore three per formula unit. According to the band structure analyses, the fourth electron transferred from the two Ba atoms is involved in more delocalized Ae1−Bi bonds, resulting in $(Sr^+)_2(Bi^-)_3 \cdot e^-$.

Longer Bi−Bi contacts (3.38 Å) are also found in the interconnected three-atom-wide ribbons in Ba_2Bi_3 and were discussed in terms of the multicenter bonds between Bi atoms with planar coordination.[16] This is not the case for the present Bi partial structure where Bi atoms have a staggered rather than planar arrangement with respect to the shorter Bi1−Bi1 contacts.

The flat bad region, which is most distinct between R and U at E_F, originates mainly from Bi-p states. The importance of such saddle points and the associated van Hove singularities in the DOS were discussed for the cuprate superconductors[27] and also for the superconducting intermetallic compounds $BaSn_5$,[23] $BaSn_3$,[28] $SrSn_3$,[29] and $SrSn_4$.[30] The simultaneous occurrence of steep bands can be interpreted in a chemical sense as an interplay between localized and

(23) Fässler, T. F.; Hoffmann, S.; Kronseder, C. *Z. Anorg. Allg. Chem.* **2001**, *620*, 2486.
(24) (a) Eisenmann, B. *Z. Naturforsch.* **1979**, *34B*, 1162. (b) *Chemistry, Structure and Bonding of Zintl Phases and Ions*; Kauzlarich, S. M., Ed.; VCH: New York, 1996; p 62.
(25) (a) Chapuis, G.; Hulliger, F.; Schmelczer, R. J. *Solid State Chem.* **1980**, *31*, 59. (b) Taylor, J. B.; Calvert, L. D.; Utsunomiya, T.; Wang, Y.; Despault, J. G. *J. Less Common Met.* **1978**, *57*, 39.
(26) Deller, K.; Eisenmann, B. *Z. Naturforsch.* **1976**, *31B*, 1023.
(27) Newns, D. M.; Krishnamurthy, H. R.; Pattnaik, P. C.; Tsuei, C. C.; Chi, C. C.; Kane, C. L. *Physica B* **1993**, *801*, 186.
(28) (a) Fässler, T. F.; Kronseder, C. *Angew. Chem.* **1997**, *109*, 2800. ; *Angew. Chem., Int. Ed. Engl.* **1997**, *36*, 2683.
(29) Fässler, T. F.; Hoffmann, S. *Z. Anorg. Allg. Chem.* **2000**, *626*, 106.
(30) Hoffmann, S.; Fässler, T. F. *Inorg. Chem.* **2003**, *42*, 8748.

delocalized bonds. Such a steep-band-flat-band scenario can be seen as a "fingerprint" in the band structure which hints for superconductivity.[31]

Conclusions

The presented results show the ability of the structure to optimize available space and bonding energy. The compounds $Sr_{2-x}Ba_xBi_3$ ($x = 0.45, 0.86, 1.08, 1.28$) represent polar intermetallics that crystallize in the structure of the nonsubstituted Sr_2Bi_3. The site preference of Ba can be explained first by the accessible cavity size and second by high bonding energies gained from strong bonding interactions between Ba and Bi atoms. On the basis of TB-LMTO-ASA results, the puzzling bonding nature of the Bi substructure can be explained by the role of Ae atoms as electron donors and as bonding partners for the Bi atoms. The dominant structural motifs are spirals of 2b-Bi atoms with short b_1 and longer b_2 distances. Increasing Ba substitution and considerable elongation of b_3 show the importance of the two shorter and the inferior importance of the longer b_3 contacts. Bond length changes in the Ba substituted samples can be interpreted as a negative chemical pressure: specific Bi−Bi bond lengths increase by the replacement of Sr by larger Ba atoms. On substitution, the opening of a pseudo gap is observed, strengthening the presence of the corresponding dominant structure motif $^1_\infty[Bi^-]$. The one extra electron is delocalized and stabilized through covalent bonding interactions between Ae and Bi, which is in contrast to Ba_2Bi_3 where the Bi−Bi multicenter contacts seem to be superior to the Ae−Bi contacts. The localized and delocalized bond scenario hints for the observed superconducting property.

Acknowledgment. The authors thank Dr. M. Opel from Walther-Meissner-Institut for Low Temperature Research (Walther-Meissner-Str. 8, D-85748 Garching) and Bele Boeddinghaus for the SQUID measurements.

Supporting Information Available: Refinement parameters for $Sr_{1.55}Ba_{0.45(2)}Bi_3$, $Sr_{1.14}Ba_{0.86(2)}Bi_3$, $Sr_{0.92}Ba_{1.08(4)}Bi_3$, $Sr_{0.72}Ba_{1.28(4)}Bi_3$ in CIF format, powder diagrams for samples Sr/Ba/Bi = $(2 - y)$:y:3 ($y = 0, 0.2, 0.4, 0.6, 0.8, 1.0, 1.2$), and table with −ICOHP values for selected Bi−Bi and Ae−Bi interactions in Sr_2Bi_3 and "Ba_2Bi_3". Plot of crystallographic compositions against loading stoichiometries and fat band representations of Bi and Sr of Sr_2Bi_3. Magnetization plots of Sr_2Bi_3 prepared in Ta and Nb ampoules.

IC7019439

(31) (a) Bäcker, M.; Simon, A.; Kremer, R. K.; Mattausch, H. J.; Dronskowski, R.; Rouxel, J. *Angew. Chem.* **1996**, *108*, 837. ; *Angew. Chem. Int. Ed.* **1996**, *35*, 752. (b) Simon, A. *Angew. Chem.* **1987**, *99*, 602. ; *Angew. Chem. Int. Ed.* **1987**, *26*, 579. (c) Simon, A. *Angew. Chem.* **1997**, *109*, 1873. ; *Angew. Chem. Int. Ed.* **1997**, *36*, 1788.